Available online at www.sciencedirect.com

SciVerse ScienceDirect

Energy Procedia 00 (2013) 000–000

Energy Procedia

www.elsevier.com/locate/procedia

SiliconPV: March 25-27, 2013, Hamelin, Germany

A Comparative Study of MWT Architectures by Means of Numerical Simulations

Paolo Magnone[a]*, Diego Tonini[b], Raffaele De Rose[a], Michel Frei[c], Felice Crupi[d], Marco Lanuzza[d], Enrico Sangiorgi[a], Claudio Fiegna[a]

[a]*ARCES-DEI, University of Bologna, Via Venezia 260, I-47521 Cesena (FC), Italy*
[b]*Applied Materials Italia s.r.l., Via Postumia Ovest 244, I-3104 Olmi di S. Biagio di Callalta (TV), Italy*
[c]*Applied Materials Inc., 3535 Garrett Dr., 95054 Santa Clara, United States*
[d]*DIMES, University of Calabria, Via P. Bucci c/o Cubo 42/C,I-87036,Rende (CS), Italy*

Abstract

In order to improve the efficiency of c-Si and mc-Si solar cells, Metal Wrap Though (MWT) architecture is investigated. In this paper we implement TCAD numerical simulations to analyze the performance of MWT cells with a point busbar or a continuous busbar at the back side. The two topologies of MWT cells are compared in both illuminated and dark conditions, aiming at understanding and comparing the resistive and recombination losses. The impact of the separation region is also studied, highlighting the degradation effect on the Fill Factor (FF) and on the efficiency in the two structures. We observe that the separation region dimension leads to a higher degradation of efficiency in case of continuous busbar.

Selection and/or peer-review under responsibility of the scientific committee of the SiliconPV 2013 conference

Keywords: MWT; solar cell, photovoltaics, numerical simulation, VIA, back contact

1. Introduction

Back contact solar cells are considered as a solution for increasing the conversion efficiency. Among the different architectures, Metal Wrap Through (MWT) [1] solar cells reduce busbar shadowing and improve Fill Factor (FF) and short-circuit current (J_{sc}) at the module level [2] by moving the busbar contact to the back side of the cell. This is accomplished with only a few new processing steps in the solar

* Corresponding author. Tel.: +39 0547 339539
E-mail address: paolo.magnone@unibo.it

cell fabrication. In particular, the current collected by the front fingers is carried towards the back busbars by means of laser drilled holes (VIAs) which are filled by conductive silver paste in order to assure enough electrical connection between front and back sides. The performance of MWT cells is significantly influenced by the back surface. Unpassivated back emitter can be a source of high recombination, especially because rear contact isolation (RCI) is required. The RCI region is created by means of laser processing, and typically leads to a large J_{02} component. Moreover, the back busbar configuration can affect the resistive and recombination losses of the MWT cell. In this work we analyze the performance of MWT solar cells using TCAD numerical simulations. Two different topologies are considered: 1) a 16-VIAs layout [3] in which a point busbar is assumed at the back side, and 2) an H-pattern layout on the top with a continuous busbar at the back side [2]. The analysis highlights the differences between the two topologies, considering both dark and illuminated conditions. The study of the impact of the separation region (i.e., between the back busbar and the p-contact) illustrates how the lateral series resistance (due to holes lateral conduction) and the high recombination region (in the separation region) affect the performance of the investigated structures.

2. Simulation Methodology

Fig. 1 contains the schematic representation of the two architectures considered in this work. Fig. 1a shows a 16-VIAs structure with a point busbar at the back, which requires a front metal grid such as a Sunweb® [4] or ECN layout [3]. Fig. 1b shows a structure with a conventional H-pattern at the front side and a continuous busbar at the back side [2]. In Sunweb® and ECN layouts, fingers are not parallel lines anymore, allowing to remove the front busbar. Therefore, we have a reduced number of VIAs (typically 16) which are far-between and with a point busbar on the back. On the other hand, in case of H-pattern at the front side, in order to reduce the width of the front busbar, a large number of VIAs is required. Since VIAs are very close each other, two or more VIAs are grouped with the same back busbar. The assumption of continuous busbar in this case is a limit consideration which highlights the influence of the separation region at the back side. The cross-section (which is the same for both structures) is reported in Fig. 1c.

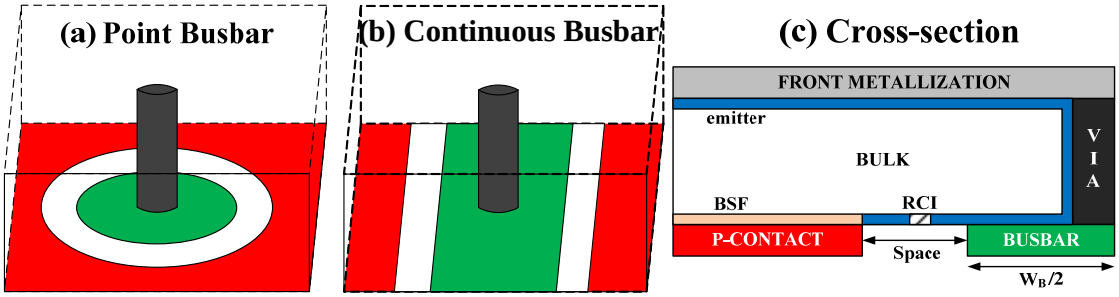

Fig. 1. MWT architectures under test: a) Point Busbar; b) Continuous Busbar; c) Cross-Section of both structures.

In order to simulate the continuous busbar structure, we performed a 2-D simulation of the cross-section in Fig. 1c (hence applying Cartesian coordinates). It is worth pointing out that this 2-D modeling approach does not represent the cylindrical shape of the VIA. On the contrary, the point busbar domain is realized by applying a cylindrical boundary condition to the cross-section of Fig. 1c and by using the VIA center as axis of rotation, thus accounting for a 3-D simulation. In both cases, Cartesian and cylindrical coordinates, the front surface is fully metallized in the simulation domain. For this reason, the front

metallization is assumed to be transparent to the incident radiation and the optical generation rate is weighted according to the front metallization fraction (3.75%). The SRV at the front interface is a weighted average between the assumed surface recombination velocities at the passivated and metallized front regions. We also considered a front-side series resistance of 0.43 Ω·cm^2 in order to account for finger, contact and emitter resistance (representative of a 3-busbar H-pattern front metal grid with a finger pitch of 2 mm, a finger sheet resistance of 2 mΩ/sq and a contact resistivity of 2 mΩ·cm^2). The VIA resistivity is assumed to be negligible. In the case of a point busbar, we assumed a structure featuring 4×4 VIAs, hence the considered element of symmetry has an area of 3.9 cm×3.9 cm. Due to the cylindrical boundary condition, the simulation domain has a circular shape while the real domain has a square shape. Therefore, the radius of the circular domain is chosen in order to obtain the same area as the square domain.

2-D and 3-D numerical simulations are performed by using a state-of-the-art TCAD device simulator [5-8]. The c-Si solar cell is 180-µm-thick and 15.6 cm×15.6 cm wide. The busbar width (W_B) is 2 mm and the bulk resistivity (ρ_{sub}) is 1.5 Ω cm. We considered an Al-p+ back surface field (BSF) modeled with a 10-µm-deep profile [9] and a 75-Ω/sq emitter profile with the typical kink-and-tail shape [10]. The fine-tuned models include the band-gap narrowing (BGN) model by Schenk to account for the effective intrinsic carrier density [11], the Auger recombination model with the parameterization adopted by Altermatt in [12], the mobility model proposed by Klaassen [13, 14], and the bulk Shockley-Read-Hall (SRH) lifetime model in boron-doped Cz-Si according to Glunz's parameterization [15] (we obtained a bulk minority carrier lifetime of about 206 µs for the considered substrate doping) and in Al-p$^+$ Cz-Si according to Altermatt's parameterization [9]. We accounted for Fermi-Dirac statistics in order to properly model highly-doped regions. We adopted the parameterization proposed by Kimmerle et al. in [16] for the surface recombination velocity (SRV) at SiNx-passivated front surface, assuming an Auger-limited lifetime in the emitter bulk and chemical phosphorus surface concentration dependence for the SRV. For the rear unpassivated regions, we assumed a surface recombination velocity (SRV) of 10^6 cm/s. Moreover, in order to highlight the effect of the laser processing, we accounted for a SRV of 10^7 cm/s in the RCI region. Optical generation rate profiles are calculated by assuming the standard AM1.5G spectrum and accounting for random pyramids textured SiN_x front surfaces.

3. Results and Discussion

3.1. Performance under illumination

In order to verify the correctness of our modeling approach, we first compare our continuous busbar cell with a similar structure analyzed in [2], by implementing the same geometrical properties and calibration of electrical parameters. The calculated dependence of the FF on the separation region width is reported in Fig. 2 and compared with simulations and experimental data reported in [2]. The curves show a similar trend. However, a shift with respect to [2] is observed. This is due to the fact that we do not account for the laser edge isolation, thus overestimating the FF, and that we probably adopt different BSF and emitter doping profiles (not reported in [2]).

Table I. Performance under illumination of the two considered structures.

Cell type	V_{oc} (mV)	J_{sc} (mA/cm^2)	*FF* (%)	η (%)
Point Busbar	634	36.97	80.86	18.94
Continuous Busbar	632	36.83	78.52	18.27

By using the simulation methodology described in section 1, we compared the properties of the two simulated solar cells under AM1.5G illumination (see Table I). No significant difference is observed in V_{oc} (open-circuit voltage) and J_{sc}, while a relevant reduction of FF is found in case of continuous busbar. Note that, for the sake of simplicity, we have assumed the same front series resistance for both types of cells. Therefore, the FF values reported in Table I do not account for differences arising from the different front metal grid.

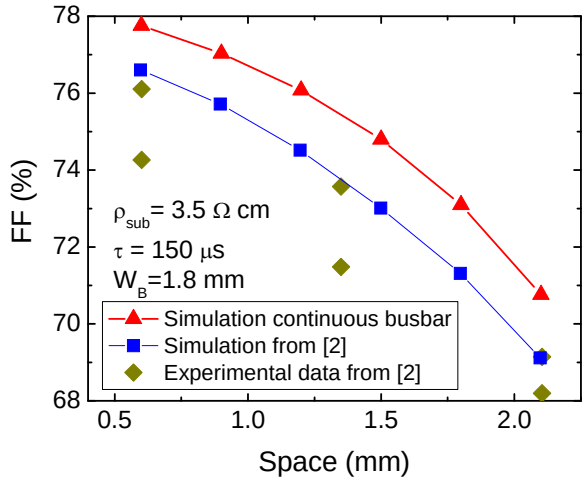

Fig. 2. Fill Factor as a function of the distance between back contacts. Simulations of continuous busbar are compared with simulation and experimental data of [2].

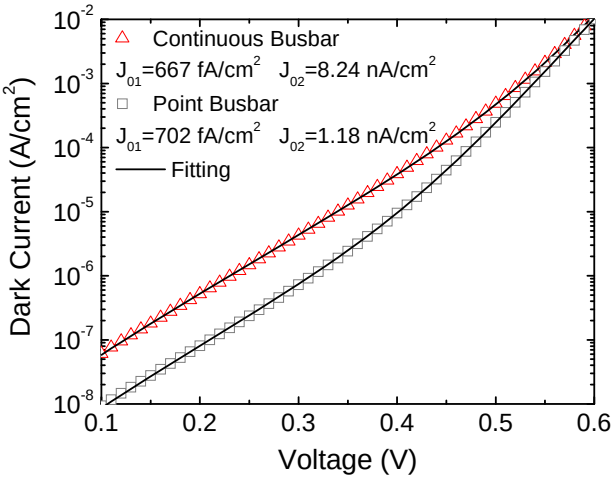

Fig. 3. Dark current in the two structures under investigation.

3.2. Dark analysis

In order to better understand the results of Table I, we also performed dark simulations for the two structures. As reported in Fig. 3, the J_{01} component is similar for both structures, since it is primarily determined by BSF, bulk and emitter recombination. This justifies the similar V_{oc} and J_{sc} values. On the

other hand, a considerably higher J_{02} is observed in the case of a continuous busbar. This result can explain the observed FF degradation. In particular, the higher J_{02} can be ascribed to the recombination current in the RCI region, which we expect to be proportional to the area occupied by the region itself. Through simple geometrical considerations, we have calculated that the area occupied by RCI region is about 6.2 times higher in case of continuous busbar as compared to the point busbar cell. It is worth noting that a similar ratio (around 7) is observed between the J_{02} currents.

3.3. Analysis of the separation between back contacts

In Fig. 4 we compare the point busbar and continuous busbar architectures as a function of the width of the separations regions between back contacts, while keeping the RCI region in the middle of the two contacts. In both cases, FF and η worsen as long as the space is increased, due to: i) the higher recombination in the unpassivated back emitter and RCI region; ii) the higher lateral series resistance; iii) the higher shunting effect between back emitter and p-contact. By comparing the two architectures, we observe that, the difference of FF and η increases as long as the separation region is increased. This means that the performance of continuous busbar cell is more influenced by the separation region than for the point busbar cell.

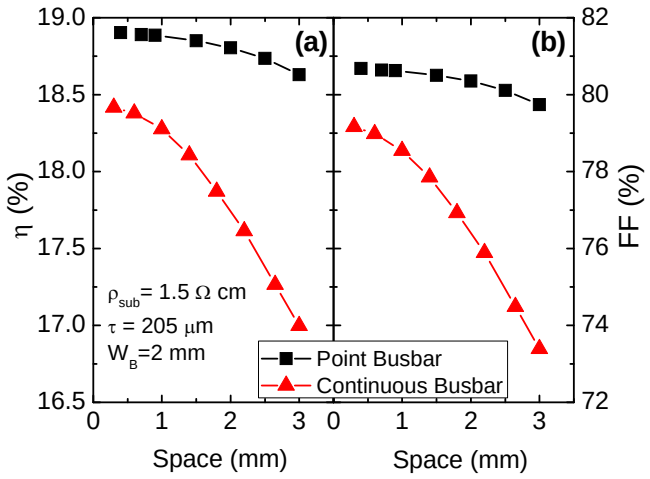

Fig. 4. Efficiency (a) and Fill Factor (b) as a function of the distance between back contacts.

Although the observed trends give useful information about the impact of the separation region, it is worth pointing out that the absolute difference of FF (between the two type of architectures) in fabricated cells can also be affected by the front resistance, which is assumed to be the same in this work, despite the different front grid layouts. Therefore, the results of this analysis have to be read only in terms of a comparative study on the degradation effect with the separation region, rather than a comparison of absolute value of FF and η between the two structures.

4. Conclusion

In this work we have compared, by means of numerical simulations, two different topologies of MWT architecture: point busbar and continuous busbar. By considering the characteristics under AM1.5G spectrum, the main difference is observed in the FF, while similar J_{sc} and V_{oc} were found. The lower FF

in the case of continuous busbar can be ascribed to the higher series resistance due to the lateral conduction of holes, to the higher shunting effect (between back emitter and p-contact) and to the higher J_{02} recombination current. As a matter of fact, the dark analysis revealed that the RCI region leads to a significant J_{02} recombination current. Since the area of the RCI region is much larger in the case of a continuous busbar (with respect to a point busbar), a larger J_{02} recombination current is observed. On the other hand a similar J_{01} recombination current was found for both structures. Finally the study on the separation region has shown how the continuous busbar efficiency is more degraded (with respect to point busbar) when the dimension of the separation region is increased.

References

[1] E. van Kerschaver, R. Einhaus, J. Szlufcik, J. Nijs, R. Mertens, "A novel silicon solar cell structure with both external polarity contacts on the back surface", *Proceedings of the 2nd World Conference on Photovoltaic Energy Conversion*, pp. 1479-82, Vienna, Austria, 1998.

[2] T. Fellmeth, K. Meyer, J. Greulich, F. Clement, D. Biro, R. Preu, M. Menkoe, D. Lahmer, H.-J. Krokoszinski, "Development and Modelling of Crystalline Silicon Based Metal Wrap Through (MWT) Solar Cells", *25th EU PVSEC*, Valencia, Spain, pp. 2201-2206, 2010.

[3] M. W. P. E. Lamers1, C. Tjengdrawira, M. Koppes, I. J. Bennett, E. E. Bende, T. P. Visser, E. Kossen, B. Brockholz, A. A. Mewe, I. G. Romijn, E. Sauar, L. Carnel, S. Julsrud, T. Naas, P. C. de Jong, A. W. Weeber, "17.9% Metal-wrap-through mc-Si cells resulting in module efficiency of 17.0%", *Progress in Photovoltaics*, Vol. 20, no. 1, pp. 62-73, 2012.

[4] Solland Solar Energy Holding BV is the owner of the registered industrial designs Sunweb®

[5] Synopsis, "Sentaurus device user guide," Version C-2009.06, 2009.

[6] R. De Rose, M. Zanuccoli, P. Magnone, M. Frei, E. Sangiorgi, C. Fiegna, "Understanding the Impact of the Doping Profiles on Selective Emitter Solar Cell by Two-Dimensional Numerical Simulation", *IEEE Journal of Photovoltaics*, vol. 3, no.1, pp. 159-167, 2013.

[7] M. Zanuccoli, R. De Rose, P. Magnone, E. Sangiorgi, C. Fiegna, "Performance Analysis of Rear Point Contact Solar Cells by Three-Dimensional Numerical Simulation". *IEEE Trans. Electron Devices*, vol. 59, no. 5, pp. 1311-1319, 2012.

[8] P. Magnone, R. De Rose, M. Zanuccoli, D. Tonini, M. Galiazzo, G. Cellere, H.-W. Guo, M. Frei, E. Sangiorgi, C. Fiegna, "Understanding the impact of double screen-printing on silicon solar cells by 2-D numerical simulations", *in Proc. 37th IEEE Photovoltaic Spec. Conf.*, pp. 2177–2180, Seattle, WA, 2011.

[9] P.P. Altermatt, S. Steingrube, Y. Yang, C. Sprodowski, T. Dezhdar, S. Koc, B. Veith, S. Herrman, R. Bock, K. Bothe, J. Schmidt, R. Brendel, "Higly Predictive Modelling of Entire Si Solar Cells for Industrial Applications", *Proc. of 24th EU PVSEC*, pp. 901-906, 2009.

[10] D. Fenning, M. Bertoni, T. Buonassisi, "Predictive modeling of the optimal phosphorus diffusion profile in silicon solar cells", *Proc. of 24th EU PVSEC*, pp. 1893-1896, 2009.

[11] A. Schenk, "Finite-temperature full random-phase approximation model of band gap narrowing for silicon device simulation", *Journal of Applied Physics*, Vol. 84, No. 7, pp. 3684-3695, 1998.

[12] P.P. Altermatt, "Models for numerical device simulations of crystalline silicon solar cells – a review", *J. Comput. Electron.*, Vol. 10, No. 3, pp. 314-330, 2011.

[13] D.B.M. Klaassen, "A unified mobility model for device simulation: I. model equations and concentration dependence", *Solid-State Electronics*, Vol. 35, No. 7, pp. 953-959, 1992.

[14] D.B.M. Klaassen, "A unified mobility model for device simulation: I. temperature dependence of carrier mobility and lifetime", *Solid-State Electronics*, Vol. 35, No. 7, pp. 961-967, 1992.

[15] S.W. Glunz, S. Rein, J.Y. Lee, W. Warta, "Minority carrier lifetime degradation in boron-doped Czochralski silicon", *Journal of Applied Physics*, Vol. 90, No. 5, pp. 2397-2404, 2001.

[16] A. Kimmerle, A. Wolf, U. Belledin, D. Biro, "Modelling carrier recombination in highly phosphorus-doped industrial emitters", *Proc. of SiliconPV 2011 Conf., Energy Procedia,* Vol. 8, pp. 275-281, 2011.